Concomitant charge-density-wave and unit-cell-doubling structural transitions in $Dy_5Ir_4Si_{10}$

M. H. Lee,[1,2] C. H. Chen,[1,2] C. M. Tseng,[3] C. S. Lue,[4] Y. K. Kuo,[5] H. D. Yang,[6] and M.-W. Chu[2,7,*]

[1]*Department of Physics, National Taiwan University, Taipei 106, Taiwan*

[2]*Center for Condensed Matter Sciences, National Taiwan University, Taipei 106, Taiwan*

[3]*Institute of Physics, Academia Sinica, Taipei 115, Taiwan*

[4]*Department of Physics, National Cheng Kung University, Tainan 701, Taiwan*

[5]*Department of Physics, National Dong Hwa University, Hualian 974, Taiwan*

[6]*Department of Physics, National Sun-Yat-Sen University, Kaohsiung 804, Taiwan*

[7]*Taiwan Consortium of Emergent Crystalline Materials, Ministry of Science and Technology, Taipei 106, Taiwan*

(Received 17 December 2013; revised manuscript received 14 April 2014; published 29 May 2014)

The tetragonal rare-earth transition-metal silicide system with three-dimensional crystallographic structure $R_5T_4Si_{10}$, where R is Dy, Ho, Er, Tm, and Lu, and T = Ir and Rh, has been shown to exhibit fascinating charge-density-wave (CDW) phase transitions, a phenomenon largely found in otherwise low-dimensional systems. In this study, we report the investigations of CDW in $Dy_5Ir_4Si_{10}$ at different temperatures using transmission electron microscopy techniques including electron diffraction and dark-field imaging. Incommensurate superlattice spots along the c axis were observed in the electron-diffraction patterns when the sample was cooled below the CDW transition temperature at ~208 K. CDW becomes commensurate with further cooling and configurations of CDW dislocations convincingly show that the CDW phase transition is accompanied by a concomitant cell-doubling crystallographic structural phase transition. Intriguingly, the cell-doubling transition is featured by a broken inversion symmetry along the c axis and a disparity in the CDW-modulation vectors with opposite signs, which gives rise to two sets of CDW domains with reversed contrasts. The profound physics underlining this notable domain-contrast behavior is discussed.

DOI: 10.1103/PhysRevB.89.195142 PACS number(s): 71.45.Lr, 64.70.Rh, 68.37.Lp, 61.44.Fw

I. INTRODUCTION

The series of ternary rare-earth–transition-metal silicides system $R_5T_4Si_{10}$, where R = Dy, Ho, Er, Tm, and Lu, and T = Ir and Rh, have been shown to exhibit various interesting phase transitions observable in the thermal and electrical transport measurements, ranging from superconductivity and long-range magnetic ordering at low temperatures (below 10 K), to charge-density waves (CDWs) at higher temperatures [1–15]. Indeed, CDW transitions are known to occur largely in low-dimensional solids where it is feasible to achieve good nesting of Fermi surfaces leading to electronic instability. The rather unexpected presence of CDW phase transitions in this class of three-dimensional $R_5T_4Si_{10}$ has drawn much attention in recent years [1–15].

The compound $Dy_5Ir_4Si_{10}$ adopts a tetragonal crystal structure (space group, $P4/mbm$) at room temperature with a = 12.577 Å and c = 4.237 Å [2]. It is generally thought that the rare-earth ions of the crystal form quasi-one-dimensional chains, which could lead to a CDW instability. Accordingly, the rare-earth network around the central site can be viewed as a channel of conductivity parallel to the chain. However, the following observations argue against the above conjectures: (1) The spacing of the rare-earth ions along the "chains" is 4.2 Å, which is too large to be considered as one dimensional. (2) The anisotropy in electrical resistivity is much smaller than typical one-dimensional systems such as $NbSe_3$ [16].

It has been suggested that precursory or concomitant structural phase transitions might facilitate the formation of the CDW state in this class of materials due to modified band structures, which might improve the nesting conditions at the Fermi surface [5,8]. In fact, it has also been substantiated that CDW transitions in this case are often accompanied by a cell-doubling structural transition [14,17].

The presence of CDW in $Dy_5Ir_4Si_{10}$ was hinted in thermal conductivity and thermoelectric power (TEP) measurements where anomalies at 208 and 165 K were found [10]. However, there was no direct evidence regarding the presence of superlattice reflections characteristic of CDW formation in $Dy_5Ir_4Si_{10}$ using diffraction techniques [10]. In this work, we report on the CDW phase transitions in $Dy_5Ir_4Si_{10}$ by selected area electron diffraction (SAED), convergent beam electron diffraction (CBED), and direct observation in real space using superlattice dark-field imaging technique in transmission electron microscopy (TEM). The dark-field images obtained from the superlattice reflections associated with the CDW phase transitions clearly show that the CDW incommensurate phase should be accurately described as discommensurate with small commensurate domains separated by sharp discommensurations (DCs) [14]. Moreover, careful SAED investigations indicate that a crystallographic cell-doubling lattice distortion occurs simultaneously with the CDW phase transition, pointing to a common occurrence in this class of materials [5]. Most surprisingly, we demonstrated by CBED that the cell-doubling transition is accompanied with the breaking of the primitive inversion symmetry along the c axis, which is closely correlated with the observation of two different sets of CDW domains with reversed contrasts.

II. EXPERIMENT

The polycrystalline sample $Dy_5Ir_4Si_{10}$ was prepared by arc-melting high-purity elements under argon atmosphere. The

*Corresponding author: chumingwen@ntu.edu.tw

detailed preparation and characterization of the samples have been reported elsewhere [2,10]. Thin specimens for TEM studies were prepared by mechanical polishing followed by ion milling at liquid nitrogen temperature and more than three samples of the $Dy_5Ir_4Si_{10}$ compound were measured to check experimental reproducibility. A JEOL 2000 FX transmission electron microscope operating at 200 kV and equipped with a low-temperature sample stage was used for the present study. The temperature accuracy of the stage has been carefully calibrated using the transition temperature of a known material, $Lu_2Ir_3Si_5$, and the temperature difference between the stage and the thermometer reading was found to be within 3 K [14,17].

III. RESULTS AND DISCUSSION

TEM examinations show that typical grain size is larger than a few micrometers, which can be treated as single crystals in the present case, since SAED patterns require only an area much smaller than 1 μm in size. Firstly, the electron-diffraction studies at room temperature [e.g., inset of Fig. 1(a)] are consistent with the primitive tetragonal structure with space group $P4/mbm$ [4,18]. Further electron-diffraction evidence of the CDW formation in $Dy_5Ir_4Si_{10}$ is shown in Figs. 1(a) and 1(b), which represent the [100] zone-axis SAED patterns taken at 100 and 190 K, respectively. The two temperatures were chosen to be below the two respective transitions at 165 and 208 K indicated in the thermal transport measurements [10]. The presence of systematic superlattice peaks in addition to the fundamental Bragg peaks is obvious, with Figs. 1(a) and 1(b) showing commensurate and incommensurate modulations, respectively. These superlattice spots are characterized by modulation wave vectors $q = (0,0,\frac{1}{4}\pm\delta)$, where δ is the temperature-dependent incommensurability with $\delta = 0$ in Fig. 1(a) and $\delta \sim 0.03$ in Fig. 1(b).

It is noted in Fig. 1 that one observes $(0,k,l)$ reflections with k = odd and l = all integers, which are symmetry forbidden to the room-temperature $P4/mbm$ structure. In addition to the CDW superlattice peaks characterized by q in Fig. 1, we also find commensurate spots systemically located at $(0,k,\frac{1}{2})$ with k = all integers and these reflections can be interpreted as different fundamental Bragg spots due to a structural phase transition involving a cell-doubling along the c axis. From the concomitant appearance of q modulations and symmetry-forbidden reflections in Fig. 1, the CDW and structural transitions in $Dy_5Ir_4Si_{10}$ should take place at the same temperature. This is different from the situation in the CDW transition of $Lu_2Ir_3Si_5$, in which the cell-doubling structural transition sets in at a slightly higher temperature than the CDW transition [17,19,20]. We first focus on the direct observation of CDW domains and domain walls using the superlattice dark-field imaging in TEM. This rather unique and powerful imaging technique has been shown to reveal the most direct details and the temperature-dependent evolution of CDW phase transitions [14,21–25].

Figures 2(a) and 2(b) show the dark-field images obtained from the commensurate CDW-modulation wave vectors $q_+ = (0,0,\frac{1}{4})$ and $q_- = (0,0,-\frac{1}{4})$ as shown in Fig. 1(a), respectively, and reveal many large dark (or otherwise bright) domains separated by sharp boundaries. Surprisingly, the domain contrast in Fig. 2(a) is reversed to that in Fig. 2(b). Considering that the order parameter of charge density in CDW systems is a pure scalar quantity, the CDW modulation generally described by the formulation of $\rho = \cos(qx + \phi)$ (ρ, charge

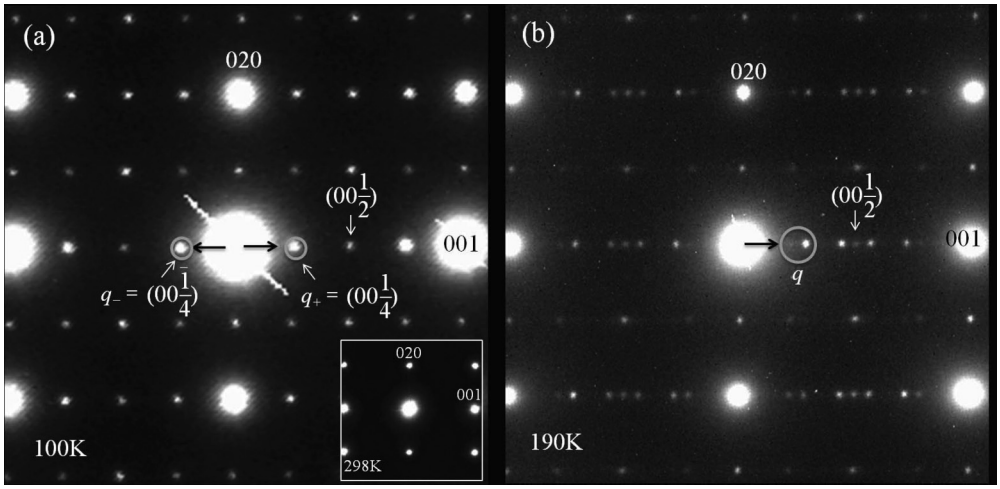

FIG. 1. (a) Electron-diffraction pattern along the [100] zone axis obtained at 100 K, which shows the commensurate superlattice spots of CDW modulations characterized by $q_+ = (0, 0, \frac{1}{4})$ and $q_- = (0, 0, -\frac{1}{4})$. The length between center to (001) Bragg peak corresponds to 1.48 Å^{-1}. The room-temperature pattern along the same projection is also shown (inset). (b) [100] zone-axis diffraction pattern taken at the same sample region as (a) at otherwise 190 K, showing the emergence of incommensurate superlattice peaks as indicated by the white circle. In (a) and (b), the systematic presence of $(0, 0, \frac{1}{2})$-type reflections indicate the cell doubling. The pair of the superlattice spots close to the $(0, 0, \frac{1}{2})$-type reflections with an incommensurability of 2δ, rather than δ characteristic of the q-modulation spots, is a result of dynamical electron-multiple scattering as confirmed by their systematic disappearance upon tilting the grain slightly away from the [100] zone. By contrast, the q-modulation spots indicated by the white circle are persistent upon the tilting. Note that the patterns taken at 100 K, 190 K, and room temperature have been subject to slightly different exposure times from one to another considering the finite dynamical range of the camera and the possible saturation of the intense central beam.

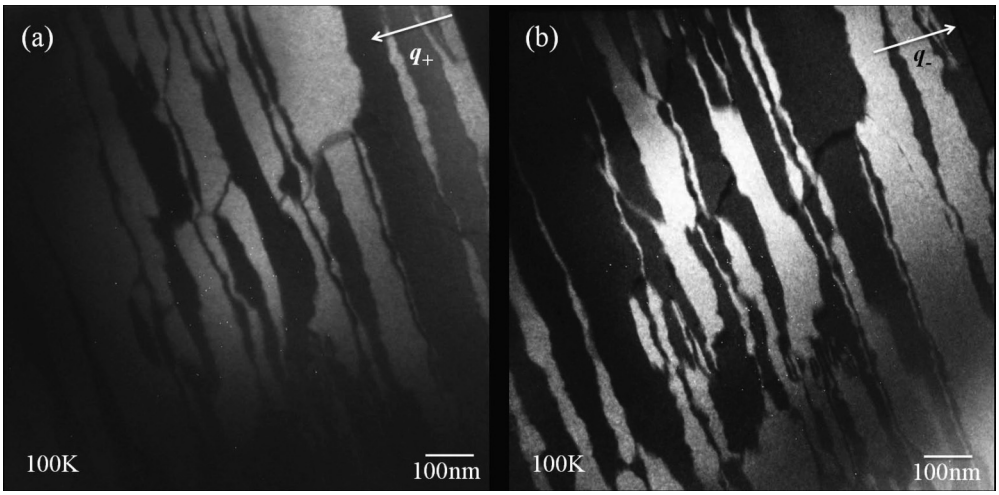

FIG. 2. (a), (b) The superlattice dark-field TEM images obtained from the respective commensurate $q_+ = (0, 0, \frac{1}{4})$ and $q_- = (0, 0, -\frac{1}{4})$ vectors in Fig. 1(a). The reversed contrasts of one to the other clearly indicate that the modulation vectors, q_+ and q_-, actually come from different domains as a result of the symmetry breaking along the c axis upon the CDW modulation.

density; q, wave vector; x, position; φ, phase) should remain invariant upon the sign reversal of q and x [26–28]. Herein, the modulation vectors of q_+ and q_- should thus be equivalent and the dark-field imaging using either q_+ or q_- would then lead to the same contrast characteristics. However, the contrast reversal shown in Fig. 2 clearly indicates that q_+ and q_- are inequivalent and q_+ and q_- arise from different domains. Note that neither chemical inhomogeneity nor impurity can be found between the two sets of domains using chemical microanalysis by energy-dispersive x-ray spectroscopy with an electron-probe size of ∼30 nm, which is also the beam diameter used in the following CBED studies (Fig. 3). The disparity in q_+ and q_- observed (Fig. 2) must come from a structural origin with intriguing coupling to the primary order parameter of charge density. We examined this structural aspect by exploiting CBED (Fig. 3), which is known to be powerful in revealing structural microdistortion and subtle symmetry breaking that cannot be easily resolved by SAED.

Figure 3(a) shows a CBED pattern taken along the [100] direction at room temperature, with high-order Laue zone (HOLZ) observed as rings centering around the enlarged zero-order Laue zone (ZOLZ) inset. A close inspection of Fig. 3(a) indicates that the characteristic features in $(0, k, l)$ and $(0, k, -l)$ reflections are identical (see the white arrowheads), pointing to the existence of a mirror symmetry perpendicular to the c axis. In Fig. 3(a), a mirror plane perpendicular to the b axis can also be observed and these mirror-symmetry elements along the [100] projection correspond to a symmetry class of $2mm$. Classically, the $4/mmm$ point group characteristic of $P4/mbm$ would give rise to a [100]-zone CBED symmetry of $2mm$ [29], indeed in agreement with our observations in Fig. 3(a). The CBED pattern taken at 98 K along the same

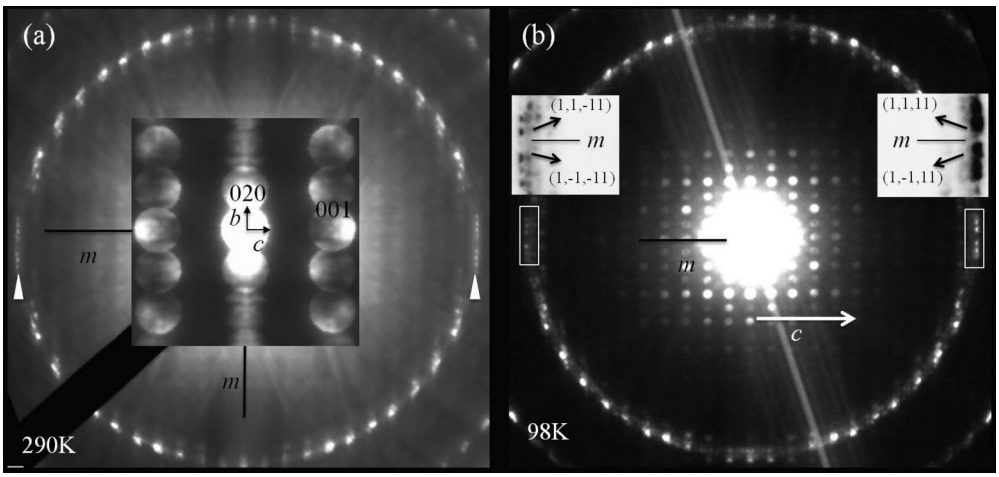

FIG. 3. CBED patterns along the [100] zone axis. (a) The reflection characteristics in the HOLZ rings and enlarged ZOLZ inset reveal the presence of two respective mirror planes, perpendicular to the b and c axes. (b) The CBED pattern acquired at low temperature, unveiling dynamical absences along the c axis as indicated by the FOLZ-reflection features in the white-block areas (for clarity, these reflections having been enlarged and shown by the reversed contrasts). These reflection features also reveal the breaking of the primitive mirror symmetry perpendicular to the c axis at low temperature, while the otherwise mirror-symmetry element perpendicular to the b axis persists.

zone axis is further shown in Fig. 3(b). Notably, only the mirror plane perpendicular to the b axis remains and the other mirror plane perpendicular to the c axis has now disappeared, as indicated by the distinct loss of mirror symmetry in the first-order Laue zone (FOLZ) features (see the rectangular white blocks and their blowups shown in reversed contrasts for clarity). In the low-temperature CDW state [Fig. 3(b)], such a symmetry-element change indicates that the concomitant cell-doubling structural transition is effectively entangled with the breaking of the primitive inversion symmetry along the c axis ($4/m$) [29]. In Fig. 3(b), the adjoining reflections of the $(1,\pm k,\pm 11)$ type are strongly excited, while the $(1,0,\pm 11)$ reflections appear to have zero intensity on the mirror line running through them (see the insets) as a result of the characteristic dynamical absence [23].

Due to the symmetry breaking along the c axis in this CDW state, q_+ and q_- become inequivalent and the dynamical-scattering nature of CBED renders the excitation intensities of associated $(1,\pm 1,-11)$ and $(1,\pm 1,11)$ readily different, with $(1,\pm 1,11)$ reflections much stronger than $(1,\pm 1,-11)$ reflections as shown in the insets of Fig. 3(b) [23,29]. Otherwise, Friedel's law, characterized by equal intensities between (h,k,l)- and $(-h,-k,-l)$-type reflections in the framework of kinematical scattering, would forbid the intensity disparity between q_+ and q_- [29,30]. Indeed, such a disparity in reflection intensities has been well established in ferroelectrics, which features the breaking of inversion centers in the unit cell, and the associated observation of contrast reversals of the 180° ferroelectric domains in $BaTiO_3$ represents a classical example [30]. Upon the careful setup of dynamical-scattering condition in $BaTiO_3$, it has been firmly shown that the inversion-symmetry breaking of the order parameter (spontaneous polarization) along the c axis can result in the breakdown of Friedel's law [30]. Using the associated q vectors with opposite signs for TEM dark-field imaging as in Fig. 2, a direct observation of 180° domains with characteristic reversed contrasts can be straightforwardly achieved [30]. What we observed in Figs. 2 and 3 altogether, with q_+ and q_- contributed by two separate sets of domains showing contrast reversals, is remarkably similar to the $BaTiO_3$ exemplification [30]. Although a microstructural model of lattice distortions is not available at the present time, it is clear that the CDW lattice modulation in $Dy_5Ir_4Si_{10}$ breaks the spatial-invariance principle and produces the domain-contrast reversal in resemblance to the 180°-twin domains in ferroelectrics [26–28,30,31]. We note that similar domain-contrast reversal has also been observed in other commensurate CDW states such as $2H$-$TaSe_2$ and $1T$-VSe_2, but detailed lattice distortions and related origin were not clearly addressed therein [21–23,32]. Later in Fig. 5, the dark-field imaging near the commensurate-to-incommensurate transition also revealed a similar contrast reversal, reaffirming the loss of inversion symmetry along the c axis in the CDW transition.

Upon cooling from room temperature, the incommensurate CDW of $Dy_5Ir_4Si_{10}$ [Fig. 1(b)] locks into a commensurate state [Fig. 1(a)] at the so-called lock-in temperature of 165 K [10]. However, detailed domain structure observations and the change of CDW superlattice reflections as a function of temperature discussed below unveil a slight difference in the lock-in transition temperature [10].

Figure 4(a) illustrates the development of the incommensurate peaks beginning at 208 K and merging into a commensurate $q = (0,0,\frac{1}{4})$ single peak at temperatures below ~143 K, with the corresponding temperature-dependent incommensurability δ plotted in Fig. 4(b). It is interesting to note in Fig. 4(b) that the lock-in temperature observed by TEM, ~143 K, is significantly different from the previous thermal transport measurements, 165 K [10], and this phenomenon could be associated with variations in local environment, such as the possible presence of strains, in the thin TEM samples [14,17,21,22].

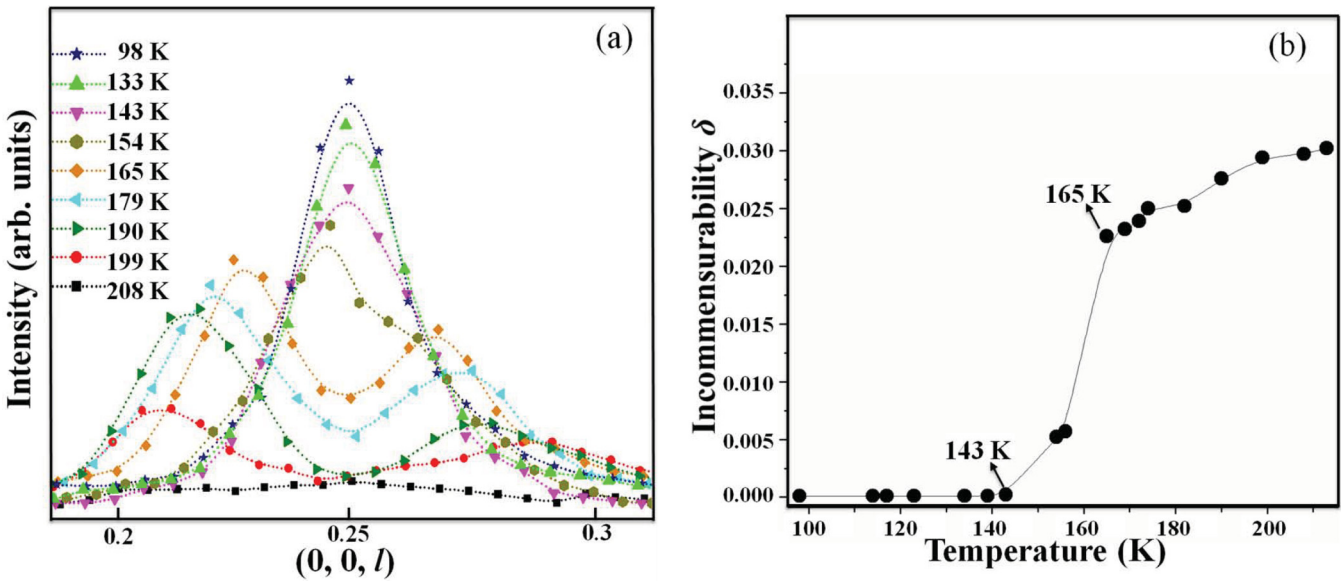

FIG. 4. (Color online) (a) The Gaussian-fitted intensity profiles across the superlattices along the c-modulation direction at various temperatures, showing the commensurate-to-incommensurate transition. (b) The value of incommensurability, δ, is varying from ~0.03 (incommensurate) to 0 (commensurate) with decreasing temperatures.

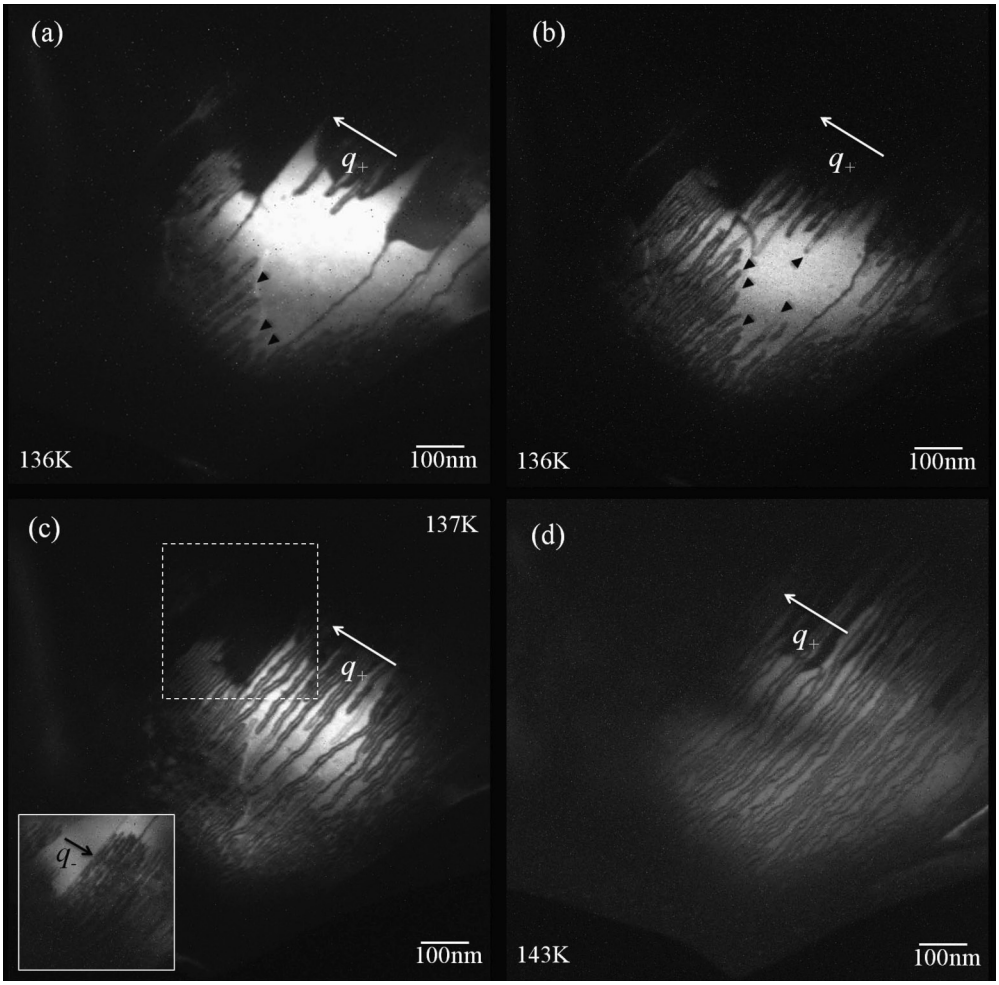

FIG. 5. Superlattice dark-field TEM images taken at various temperatures from the same area, which show the residual DC domain walls in the commensurate phase (a) and the presence and movement of the CDW dislocations in (b)–(d). All the images were taken from the satellite peaks located at $(4, 0, \frac{1}{4}\pm\delta)$. It is noted that two DCs are always required to form a CDW dislocation. A few corresponding dislocations marked by arrows in (a) and (b) seem to move at a slower speed than the others. Upon further warming, the density of the DCs has rapidly increased as shown in (d). Inset in (c) shows the dark-field imaging of the dotted region using the q vector with an otherwise opposite sign. The contrast in the inset is reversed to that using q_+.

Figures 5(a)–5(d) show a series of dark-field images obtained from the CDW satellite peaks at several different temperatures near the commensurate-to-incommensurate CDW transition of ∼143 K on warming and the dark lines therein are DC domain walls, where the CDW phase changes rapidly [14,17]. As the temperature approach the transition temperature, DCs are found to nucleate within the commensurate domain [black arrows, Fig. 5(a)] and the nearly incommensurate state in Fig. 5(d) is characterized by the presence of small commensurate domains separated by DCs, which has been known as a discommensurate phase [14,17]. It is well known that nucleation, growth, and annihilation of DCs play the most critical role for the commensurate-to-incommensurate transition and the physics of the transition has been well described based on the Landau theory in the early literature [26,31,33]. Furthermore, it is obvious that the DC domain walls start to appear near the edge of the sample at ∼136 K. It deserves mentioning that there exists a discernible change in the TEP results of the material at ∼136 K [10]. Indeed, the TEP measurements are known to be very sensitive to the changes in the Fermi-level density of states (DOS) [10], and this would suggest that the commensurate-to-incommensurate transition observed by TEM is accompanied by a notable change of DOS near the Fermi surface. Further experiments will be required to elucidate the ∼136 K transition, which is a separate issue on its own. It should be mentioned that a close inspection of the SAED pattern corresponding to Fig. 5 reveals a nearly vanishing incommensurability, δ, for the otherwise broad superlattice spots [see Fig. 4(a), 133 K, for instance], although nonzero δ would be generally expected for CDW phases with appreciable DCs as in Fig. 5. The vanishing δ herein, in effect, arises from the strong intensity of the $(0,0,\frac{1}{4})$-type reflections of the commensurate domains, which buries the subtle incommensurability in the intense commensurate superlattices and leads to the broad width of the modulation peaks.

In addition, nodes at which DCs join together are known as CDW dislocations and many CDW dislocations are evident in Figs. 5(a)–5(d) (black arrows). It is clear that every CDW dislocation involves only two DCs. The fact that two DCs

are always needed in the present case to form a CDW dislocation demonstrates that the phase shift across a DC is π and the modulation wave vector should be of the type $q = (0,0,\frac{1}{2})$ instead of $q = (0,0,\frac{1}{4})$, which would otherwise require four DCs to merge at a CDW dislocation node. The c-axis cell-doubling structural phase transition, which simultaneously occurs with CDW, would automatically lower the order of commensurability (n) from $n = 4$ to $n = 2$ and, hence, requires only two DCs to form a CDW dislocation. Nucleation and growth of the CDW dislocations are usually the most fascinating aspect of the entire evolution process of various CDW phases. With increasing temperature [Figs. 5(a)–5(d)], while new CDW dislocations are being nucleated, the existing CDW dislocations continue to move and result in further lengthening and increasing density of DCs. The CDW dislocations are found to move with different speeds, which could reflect the local variations of strains and pinning strength fluctuations along the path they encounter. A few CDWs marked by arrows in Fig. 5(b) seem to move much more slowly than others and are still visible in Fig. 5(c). It is noted that the original residual DCs observed at lower temperatures as shown in Fig. 5(a) remain largely motionless and unchanged in the initial warming process, which signifies the strong pinning effect of the CDWs. We note also that annihilation of the CDW dislocations also plays an important role during the thermal evolution of the phase transition [14,17]. The evolution of the commensurate-to-incommensurate phase transition is entirely controlled by the process of nucleation, growth, and annihilation of the CDW dislocations and the commensurate phase can be satisfactorily understood as a transition underlined by the disappearance of DCs from the incommensurate phase [26,31,33]. Following this latter established conception, the dark-field imaging of the incommensurate phase using q_- should then lead to the same contrast-reversal phenomenon as in Fig. 2. In Fig. 5(c), the exploitation of q_- for the imaging (inset) indeed results in a contrast reversal compared to q_+. We show in the present work that detailed investigation in TEM dark-field technique can reveal profound details about CDW.

Moreover, it deserves mentioning that the recent study of two-dimensional $1T$-$TiSe_2$ using scanning tunneling microscopy revealed intricate variations in the intensity of charge-density superlattice reflections, with the respective intensities of the three characteristic commensurate q modulations diminishing in the order of a clockwise or counterclockwise pattern [27]. Such a helical-like intensity variation breaks the parity in q and further implies the emergence of chiral CDW along the common projected vector of the q's [27,28]. In Fig. 1(b), we also observed a subtle intensity fluctuation of the superlattice spots and Fig. 5(c) unveils the accompanied disparity in q. It seems plausible that the subtle disparity of superlattice reflections in $Dy_5Ir_4Si_{10}$ could arise from the handedness of the CDW modulations, resulting naturally in two types of domains as we have discussed. $Dy_5Ir_4Si_{10}$ features, however, only one single set of q and whether CDW with a handedness could emerge along this q vector would require additional theoretical and experimental verifications in the future, such as the polarization-dependent transient reflectivity also exploited in the study of $1T$-$TiSe_2$ [27]. Indeed, the subject of chiral CDW in three-dimensional crystalline systems represents an intriguing and largely unexplored area.

IV. CONCLUSION

The CDW transition and domain characteristics of $Dy_5Ir_4Si_{10}$ were thoroughly investigated on the basis of electron-diffraction studies. Using superlattice dark-field imaging, configurations of the corresponding CDW dislocations, where two, instead of four, DCs were found to form a dislocation node, convincingly establish that the CDW transition is accompanied with a concomitant cell-doubling structural transition. The careful CBED investigations of this low-temperature CDW phase revealed a broken symmetry along the c axis, leading to the observation of the intriguing phenomenon of two different sets of CDW domains with reversed contrasts in this class of materials. Moreover, the CDW dislocations appear to occur at ~136 K rather than the generally accepted lock-in transition temperature of 165 K, suggesting an associated change in DOS near the Fermi surface. Indeed, an electronic anomaly at ~136 K has been previously pointed out using macroscopic thermoelectric measurements without knowing the profound details and this work provides useful microscopic details for the future elaboration of the problem.

[1] R. N. Shelton, L. S. Hausermann-Berg, P. Klavins, H. D. Yang, M. S. Anderson, and C. A. Swenson, Phys. Rev. B **34**, 4590 (1986).
[2] H. D. Yang, P. Klavins, and R. N. Shelton, Phys. Rev. B **43**, 7688 (1991).
[3] K. Ghosh, S. Ramakrishnan, and G. Chandra, Phys. Rev. B **48**, 4152 (1993).
[4] B. Becker, N. G. Patil, S. Ramakrishnan, A. A. Menosvky, G. J. Nieuwenhuys, J. A. Mydosh, M. Kohgi, and K. Iwasa, Phys. Rev. B **59**, 7266 (1999).
[5] F. Galli, S. Ramakrishnan, T. Tanigushi, G. J. Nieuwenhuys, J. A. Mydosh, S. Geupel, J. Ludecke, and S. Van Smaalen, Phys. Rev. Lett. **85**, 158 (2000).
[6] Y. K. Kuo, C. S. Lue, F. H. Hsu, H. H. Li, and H. D. Yang, Phys. Rev. B **64**, 125124 (2001).
[7] C. S. Lue, F. H. Hsu, H. H. Li, H. D. Yang, and Y. K. Kuo, Physica C **364–365**, 243 (2001).
[8] F. Galli, R. Feyerherm, R. W. A. Hendrikx, E. Dudzik, G. J. Nieuwenhuys, S. Ramakrishnan, S. D. Brown, S. van Smaalen, and J. A. Mydosh, J. Phys.: Condens. Matter **14**, 5067 (2002).
[9] C. S. Lue, Y. K. Kuo, F. H. Hsu, H. H. Li, H. D. Yang, P. S. Fodor, and L. E. Wenger, Phys. Rev. B **66**, 033101 (2002).
[10] Y. K. Kuo, F. H. Hsu, H. H. Li, H. L. Huang, C. W. Huang, C. S. Lue, and H. D. Yang, Phys. Rev. B **67**, 195101 (2003).

[11] S. van Smaalen, M. Shaz, L. Palatinus, P. Daniels, F. Galli, G. J. Nieuwenhuys, and J. A. Mydosh, Phys. Rev. B **69**, 014103 (2004).
[12] H. L. Liu, G. S. Wu, J. L. Her, and H. D. Yang, Phys. Rev. B **72**, 205102 (2005).
[13] F. Bondino, E. Magnano, E. Carleschi, M. Zangrando, F. Galli, J. A. Mydosh, and F. Parmigiani, J. Phys.: Condens. Matter **18**, 5773 (2006).
[14] C. M. Tseng, C. H. Chen, and H. D. Yang, Phys. Rev. B **77**, 155131 (2008).
[15] Y. K. Kuo, Y. Y. Chen, L. M. Wang, and H. D. Yang, J. Magn. Magn. Mater. **282**, 338 (2004).
[16] K. Tsutsumi, S. Takayanagi, K. Maezawa, and H. Kitazawa, J. Alloys Compd. **453**, 55 (2008).
[17] M. H. Lee, C. H. Chen, M.-W. Chu, C. S. Lue, and Y. K. Kuo, Phys. Rev. B **83**, 155121 (2011).
[18] C. Opagiste, M. Leroux, P. Rodière, G. Garbarino, S. Pairis, P. Bordet, and P. Lejay, J. Cryst. Growth **312**, 3204 (2010).
[19] Y. Singh, D. Pal, S. Ramakrishnan, A. Awasthi, and S. Malik, Phys. Rev. B **71**, 045109 (2005).
[20] Y. K. Kuo, K. M. Sivakumar, T. M. Su, and C. S. Lue, Phys. Rev. B **74**, 045115 (2006).
[21] C. H. Chen, J. M. Gibson, and R. M. Fleming, Phys. Rev. Lett. **47**, 723 (1981).
[22] C. H. Chen, J. M. Gibson, and R. M. Fleming, Phys. Rev. B **26**, 184 (1982).
[23] K. K. Fung, S. McKernan, J. W. Steed, and J. A. Wilson, J. Phys. C **14**, 5417 (1981).
[24] C. H. Chen and R. M. Fleming, Phys. Rev. B **29**, 4811 (1984).
[25] Y. Koyama, Z. P. Zhang, and H. Sato, Phys. Rev. B **36**, 3701 (1987).
[26] W. L. McMillan, Phys. Rev. B **14**, 1496 (1976).
[27] J. Ishioka, Y. H. Liu, K. Shimatake, T. Kurosawa, K. Ichimura, Y. Toda, M. Oda, and S. Tanda, Phys. Rev. Lett. **105**, 176401 (2010).
[28] J. van Wezel, Europhys. Lett. **96**, 67011 (2011).
[29] D. B. Williams and C. B. Carter, *Transmission Electron Microscopy* (Plenum Press, New York, 1996), Chap. 21.
[30] M. Tanaka and G. Honjo, J. Phys. Soc. Jpn. **19**, 954 (1964).
[31] W. L. McMillan, Phys. Rev. B **12**, 1187 (1975).
[32] D. J. Eaglesham, R. L. Withers, and D. M. Bird, J. Phys. C **19**, 359 (1986).
[33] R. N. Bhatt and W. L. McMillan, Phys. Rev. B **12**, 2042 (1975).